Available online at www.sciencedirect.com

SciVerse ScienceDirect

Geochimica et Cosmochimica Acta 75 (2011) 6690–6704

Geochimica et Cosmochimica Acta

www.elsevier.com/locate/gca

Thallium isotopes in early diagenetic pyrite – A paleoredox proxy?

Sune G. Nielsen [a,b,*], Matt Goff [a], Stephen P. Hesselbo [a], Hugh C. Jenkyns [a], Doug E. LaRowe [c,d], Cin-Ty A. Lee [e]

[a] Department of Earth Sciences, University of Oxford, South Parks Road, Oxford OX1 3AN, UK
[b] Department of Geology and Geophysics, Woods Hole Oceanographic Institution, Woods Hole, 02543 MA, USA
[c] School of Earth and Atmospheric Science, Georgia Institute of Technology, Atlanta, GA 30332-0340, USA
[d] Faculty of Geosciences, Department of Earth Science – Geochemistry, Utrecht University, P.O. Box 80021, 3508 TA Utrecht, The Netherlands
[e] Department of Earth Science, MS-126, Rice University, 6100 Main St., Houston, TX 77005, USA

Received 28 October 2010; accepted in revised form 28 July 2011; available online 4 August 2011

Abstract

This paper presents the first study of Tl isotopes in early diagenetic pyrite. Measurements from two sections deposited during the Toarcian Ocean Anoxic Event (T-OAE, ~183 Ma) are compared with data from Late Neogene (<10 Ma) pyrite samples from ODP legs 165 and 167 that were deposited in relatively oxic marine environments. The Tl isotope compositions of Late Neogene pyrites are all significantly heavier than seawater, which most likely indicates that Tl in diagenetic pyrite is partially sourced from ferromanganese oxy-hydroxides that are known to display relatively heavy Tl isotope signatures. One of the T-OAE sections from Peniche in Portugal displays pyrite thallium isotope compositions indistinguishable from Late Neogene samples, whereas samples from Yorkshire in the UK are depleted in the heavy isotope of Tl. These lighter compositions are best explained by the lack of ferromanganese precipitation at the sediment–water interface due to the sulfidic (euxinic) conditions thought to be prevalent in the Cleveland Basin where the Yorkshire section was deposited. The heavier signatures in the Peniche samples appear to result from an oxic water column that enabled precipitation of ferromanganese oxy-hydroxides at the sediment–water interface.

The Tl isotope profile from Yorkshire is also compared with previously published molybdenum isotope ratios determined on the same sedimentary succession. There is a suggestion of an anti-correlation between these two isotope systems, which is consistent with the expected isotope shifts that occur in seawater when marine oxic (ferromanganese minerals) fluxes fluctuate.

The results outlined here represent the first evidence that Tl isotopes in early diagenetic pyrite have potential to reveal variations in past ocean oxygenation on a local scale and potentially also for global oceans. However, much more information about Tl isotopes in different marine environments, especially in anoxic/euxinic basins, is needed before Tl isotopes can be confidently utilized as a paleo-redox tracer.

1. INTRODUCTION

Through Earth's history, oxygenation of the oceans has played a central role in the evolution of life and has also, through the intimate link with the carbon cycle, been a factor in controlling climate. Several geochemical proxies are useful indicators of past marine oxygen levels, for example abundances of total organic carbon (TOC) and redox-sensitive trace metals (e.g. Fe, Re, U, Mo and V) in sediments (Emerson and Huested, 1991; Kendall et al., 2010) as well as nitrogen isotope ratios measured in organic carbon (Altabet and Francois, 1994). Most of these proxies, however, are better suited to studies of local or regional redox conditions either because the marine residence time of the element may be too short or because the elemental

* Corresponding author at: Department of Earth Sciences, University of Oxford, South Parks Road, Oxford OX1 3AN, UK. Tel.: +44 1865272027.
E-mail address: sune.nielsen@earth.ox.ac.uk (S.G. Nielsen).

0016-7037/$ - see front matter © 2011 Elsevier Ltd. All rights reserved.
doi:10.1016/j.gca.2011.07.047

flux into the sediment is not exclusively controlled by large-scale or global seawater oxygenation.

With the advent of multiple collector inductively coupled plasma mass spectrometers (MC-ICPMS) it has become possible to study the stable isotope systematics of redox-sensitive trace metals (Beard et al., 1999; Siebert et al., 2003; Stirling et al., 2007; Miller et al., 2009; Nielsen et al., in press). In theory, stable isotope variations of redox-sensitive trace metals with long marine residence times offer the opportunity to look past local effects and provide information related to changes in average oxygenation of the global oceans. Recently, this potential has prompted the emergence of new redox-sensitive metal isotope proxies such as molybdenum (Mo) and uranium (U), which have produced the first attempts to determine global levels of anoxia during ocean anoxic events (OAEs) (Archer and Vance, 2008; Pearce et al., 2008; Montoya-Pino et al., 2010) and these have suggested that OAE2 (at the Cenomanian–Turonian boundary, ~93 Ma) and T-OAE (Toarcian oceanic anoxic event, ~183 Ma) coincided with threefold and tenfold expansions, respectively, of the area of anoxic sediment deposition.

Another element with potential to reveal information about past oceanic anoxia is thallium (Tl), which has two isotopes, ^{203}Tl and ^{205}Tl, that are both stable. The distribution of Tl in natural environments on Earth is controlled in part by its large ionic radius, which is akin to the alkali metals potassium (K), rubidium (Rb) and cesium (Cs) (Wedepohl, 1974; Shannon, 1976; Heinrichs et al., 1980). Its large ionic radius renders Tl highly incompatible during igneous processing and it hence concentrates in the continental crust (Shaw, 1952). Thallium can take on two different valence states: Tl^{+} and Tl^{3+}. The oxidized form is uncommon in natural environments because of the high redox potential, but it is likely that this form of Tl plays a significant part in the observed strong adsorption onto authigenic ferromanganese phases and clay minerals in aqueous environments (Matthews and Riley, 1970; McGoldrick et al., 1979; Hein et al., 2000; Turner et al., 2010).

Modern seawater is depleted in ^{203}Tl compared with average continental crust and mantle, and the isotopic composition is homogenous (Rehkämper et al., 2002; Nielsen et al., 2006) with a marine residence time of ~20 kyr (Rehkämper and Nielsen, 2004; Baker et al., 2009) (Fig. 1). Temporal changes of the marine Tl isotope ratio are most likely controlled solely by the ratio between the two marine output fluxes (Nielsen et al., 2009a), which display highly fractionated and contrasting Tl isotope compositions (Rehkämper et al., 2002; Rehkämper et al., 2004; Nielsen et al., 2006). The two output fluxes are (1) scavenging by authigenic ferromanganese (Fe–Mn) oxy-hydroxides and (2) uptake of Tl during low temperature (low-T) alteration of oceanic crust. All types of authigenic Fe–Mn deposits (hydrogenous/diagenetic nodules and crusts and coatings on pelagic sediments) except high-temperature hydrothermal precipitates are enriched in the heavy isotope (^{205}Tl) (Rehkämper et al., 2002; Rehkämper et al., 2004). The isotope fractionation appears to be related to surface oxidation of Tl when adsorbed onto low-temperature Mn oxides (Bidoglio et al., 1993), while isotope fractionation is absent during Tl adsorption onto the predominantly high-temperature Mn oxide todorokite (Peacock et al., 2009). Altered oceanic crust exhibits light Tl isotope compositions with the shallowest portions characterized by the highest Tl concentrations and lightest isotope compositions (Coggon et al., 2009; Nielsen et al., 2006). The mechanism controlling the incorporation of isotopically light Tl

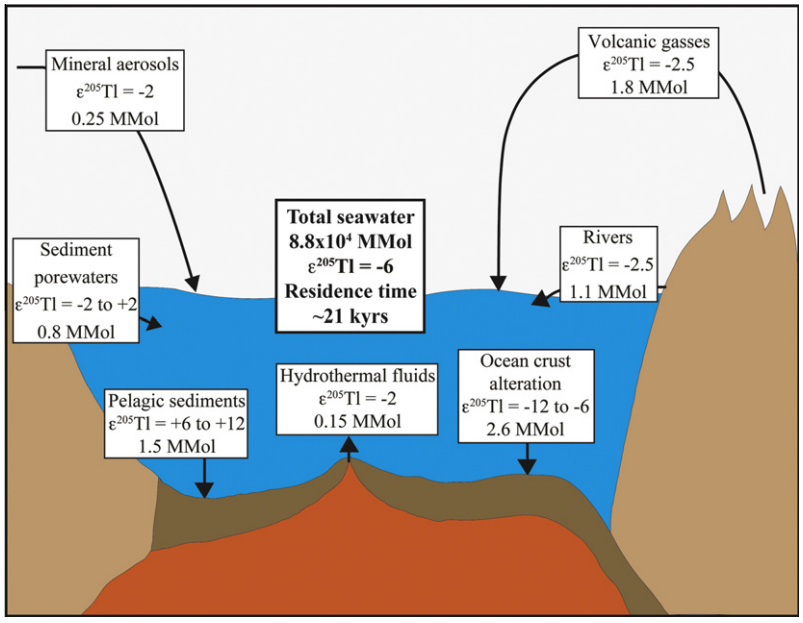

Fig. 1. Modern marine thallium isotope cycle. Each box represents the magnitude of a major flux of Tl to the global ocean in millions of moles per year, MMol, and a summary of its typical isotopic composition, ε^{205}Tl. The data for individual fluxes are compiled from Rehkämper et al. (2002, 2004), Nielsen et al. (2005, 2006), Baker et al. (2009) and Nielsen and Rehkämper (2011).

during alteration of oceanic crust is yet to be explained, but could be kinetic in nature (Nielsen and Rehkämper, 2011). Thallium is supplied to the oceans by rivers, high-temperature hydrothermal fluids, volcanic emanations, mineral aerosols, and pore-water fluxes from continental-margin sediments, all of which show essentially identical Tl isotope compositions (Fig. 1). Importantly, Tl isotopes do not exhibit any resolvable overall fractionation during any of the processes supplying Tl to the ocean (Nielsen et al., 2005, 2006; Baker et al., 2009; Nielsen et al., 2009a). Input fluxes are, therefore, unlikely to drive significant changes in the Tl isotope composition of seawater (Nielsen et al., 2009a).

From the perspective of oceanic anoxia, the marine Tl isotope cycle is interesting because authigenic Fe–Mn oxy-hydroxides only precipitate in a relatively oxygenated environment. Therefore, it might be expected that widespread ocean anoxia would result in significantly diminished Tl outputs associated with Fe–Mn minerals, resulting in heavier seawater Tl isotope compositions. The magnitude of such changes might, however, be difficult to predict because the general mechanism controlling the Tl isotope fractionation of low-temperature alteration of oceanic crust is currently unknown.

Here, we report the first investigation of the utility of Tl isotopes as a paleoredox proxy. To this end, we have measured the Tl isotope composition of early diagenetic pyrite in shales collected at Port Mulgrave in Yorkshire, North England and Peniche, Portugal that both record the T-OAE. The T-OAE is characterized by a diagnostic negative carbon-isotope excursion in carbonate and organic matter interrupting an overall positive trend (Jenkyns and Clayton, 1997; Hermoso et al., 2009a). The excursion has now been recognized in both the northern and southern hemispheres (Hesselbo et al., 2007; Al-Suwaidi et al., 2010; Jenkyns, 2010), which clearly documents the global nature of this event. The Yorkshire section was deposited in a geographically restricted segment of the Jurassic north European seaway where sediments include coarse- and fine-grained clastics and limestones (Hesselbo and Jenkyns, 1995; Jenkyns, 2010); the Peniche section was deposited on an open shelf and is dominated by clay-rich hemipelagic carbonates interbedded with sandstone turbidites (Hesselbo et al., 2007; Hermoso et al., 2009b).

In order to put our results into a modern framework we compare the measurements of Toarcian samples with a number of pyrite specimens separated from sediment cores recovered during ODP leg 165 at site 1000A in the Caribbean (0.3–0.8% TOC) and ODP leg 167 at sites 1020B (0.4–1.2% TOC) and 1021B (0–0.6% TOC) in the Northeast Pacific on the continental shelf off Oregon.

Early diagenetic pyrite precipitates from reducing sediment pore waters, which source their major and trace elements from seawater and minerals such as Fe and Mn oxides and hydroxides that are soluble under reducing conditions (Berner, 1984; Canfield et al., 1992). Hence, the Tl isotope composition of early diagenetic pyrite should depend to some degree on the isotope composition of seawater as well as the make-up of the components that supplied Tl to the pore water from which the pyrite precipitated.

2. SAMPLES AND METHODS

2.1. Sample descriptions and pyrite separation

The reason for choosing to measure pyrite instead of bulk samples is that the Tl concentration of detrital sedimentary grains is relatively high at around 0.2–0.7 ppm (Matthews and Riley, 1970; Heinrichs et al., 1980; Rehkämper et al., 2004). Since we are only interested in the labile Tl pool, which is ultimately sourced from seawater, it was necessary to perform a relatively efficient separation of pyrite from the host sediment. It is important to note that some of the pyrite from Yorkshire may be framboidal in origin, some of which is formed in the water column instead of in the sediment. However, framboidal pyrite is most commonly <10 μm in diameter (Wilkin and Barnes, 1997). Because the grain sizes we work with here are on the order of mm, we believe that only an insignificantly small fraction of the pyrite investigated here is framboidal in origin. This distinction is important because we want to be able to compare directly the Tl isotope composition of pyrite formed in the sediment at the two T-OAE sites. Authigenic framboidal pyrite may not be characterized by the same isotope composition as early diagenetic pyrite.

The samples from Port Mulgrave were collected with a stratigraphic resolution of ~20 cm or wherever macroscopic pyrite was visible in the exposed sediments. Hand specimens were disaggregated with a hammer and mm- to cm-sized chunks of pyrite-rich material were manually separated. The chunks were further crushed, sieved and rinsed in water and ethanol, before 0.5–2 mm sized crystals of pure pyrite were separated using a binocular microscope. Prior to digestion, samples were ultrasonicated several times in MQ water and dilute HCl to remove any potential surface contamination and sedimentary particles still associated with the pyrite. Twenty-three samples were analyzed, collected through a 6.5 m stratigraphic section covering the negative carbon-isotope anomaly of the T-OAE.

Samples from Peniche did not contain large macroscopic pyrite minerals. In these samples, pyrite was finely disseminated within fossilized wood that occurs commonly throughout the ~37 m thick T-OAE section. The pyrite associated with the wood is most likely of a marine origin as terrestrial pyrite is rare due to the low sulfate contents of fresh water. Additionally, the fact that the fossil wood C-isotope stratigraphy of Hesselbo et al. (2007) is consistent with the bulk carbonate record strongly suggests that the wood was not extensively reworked and probably transported from the terrestrial to the marine environment in a relatively short period of time.

Attempts to separate pyrite mechanically from fossilized wood proved to be impractical for more than a few samples, and it was decided to process the pyritized wood directly. Chips of wood (mm-sized) were therefore picked with tweezers and ultrasonicated for 30 min in MQ water to remove sedimentary particles before digestion. A total of 29 samples covering the entire T-OAE as well as some of the time periods pre- and post-dating the event were investigated.

The geologically young (Late Neogene) pyrite samples were even more difficult to isolate because the sediment

cores had experienced significant oxidation while in storage since they were recovered in the late 1990's. Sediment cores containing large yellow-red patches, which had also originally been described as containing abundant pyrite, were targeted (Sigurdsson et al., 1997; Lyle et al., 1998a,b). The sediments were dried, sieved and washed and thereafter rusty aggregates were picked under binocular microscope. Sample 165-1020B-3H-2, 68–70 cm contained some dark grains that resembled pyrite, which were not entirely oxidized. Therefore two separate samples were isolated, one of which contained the least oxidized grains and one that was similar to the other reddish oxidized pyrite samples.

Sample 165-1021B-15H-3, 89–91 cm was a piece of pyritized wood, which was treated in the same manner as were the Peniche samples. Sample 201-1227D-4H-2, 40–42 cm was a pyrite-free sample, which was analyzed in order to compare with samples that contained pyrite. The core from Hole 1227D has high TOC (1.2–10.6%) and pyrite is present in some sections (D'Hondt et al., 2003). Via macroscopic inspection we determined that there was no appreciable pyrite in the sample analyzed.

2.2. Chemical treatment of samples

After ultrasonification, the Port Mulgrave samples were digested in a 1:1 mixture of distilled concentrated HNO_3 and HCl with small amounts of MQ water added to contain the exothermic reaction of pyrite dissolution. Samples were then evaporated to dryness and dissolved in 1 M HCl. Small amounts of residual solids still remained after dissolution, which most likely was silicate material. These residues were discarded as they could potentially contaminate the pyrite-bound Tl.

Due to the disseminated nature of the Peniche pyrite, a somewhat less aggressive digestion technique was employed. The pyritized wood was submerged in ~5 ml 3 M HNO_3 overnight at ~130 °C. Thereafter, samples were evaporated to dryness and re-dissolved in an appropriate volume (2-5 ml) of 1 M HCl. Significant amounts of organic material and sedimentary particles were still present after this treatment. Similarly to the Port Mulgrave samples, these solids were discarded. Because it was thought that the organic material from the fossilized wood could potentially create artificial isotopic effects in the Peniche samples, one sample (PW69) with adequate material was also processed mechanically whereby pyrite was isolated by crushing, sieving and handpicking under binocular microscope. In this way we could evaluate whether the two techniques of pyrite separation yielded consistent results.

The Late Neogene pyrite samples were digested in 2 ml ~8 M HNO_3 overnight at ~130 °C. Thereafter, samples were evaporated to dryness and re-dissolved in 1 M HCl. After acid digestion, a detrital residue was again present, which was discarded.

2.3. Chemical separation of thallium and mass spectrometry

After dissolving samples in 1 M HCl, ~50–100 μl of MQ water saturated with Br_2 was added in order to oxidize all Tl to the trivalent state (Rehkämper and Halliday, 1999). Thallium was separated from dissolved sample matrix in teflon mini-columns with 100 μl resin beds using a previously described technique (Nielsen et al., 2004). For the Neogene pyrite, the sample matrix was also collected for subsequent major- and trace-element analysis. These matrix samples were evaporated on a hotplate and re-dissolved in 100 ml 2% HNO_3 with a trace of HCl in order to keep iron stable in solution.

Major- and trace-element concentrations, except for Tl, were measured on a Thermo Finigan Element2 ICP-MS at Rice University using In as an internal standard and calibrated against the USGS rock standards BCR-2, BHVO-2 and BIR-1. Major and some trace elements (Fe, Mg, Ca, Na, K, Mn, Co, Ni and Cu) were analyzed in medium mass resolution mode, whereas the remaining trace elements (Li, Rb, Sr, Cs, Ba, Hf, Pb, Th and U) were analyzed in low-mass resolution mode. Trace-element concentrations are accurate and precise to better than ±10% (1sd). Thallium concentrations were calculated assuming 100% yields during Tl separation for isotope analysis (Nielsen et al., 2004). A known quantity of NIST SRM 981 Pb was added to the sample Tl and the measured $^{205}Tl/^{208}Pb$ ratios were converted into Tl abundances by assuming that Tl ionises 5% more efficiently than does Pb. These concentrations are precise and accurate to about ±10% (1sd).

Thallium isotope ratios were measured at the University of Oxford on a Nu Plasma HR-MC-ICPMS operated in standard low-resolution mode. Previously described techniques that utilize both external normalization to NIST SRM 981 Pb and standard-sample bracketing were applied for mass-bias correction (Rehkämper and Halliday, 1999; Nielsen et al., 2004). Thallium isotope compositions are reported relative to the NIST SRM 997 Tl standard in parts per 10,000 such that

$$\varepsilon^{205}\mathrm{Tl} = 10,000 \times \left(^{205}\mathrm{Tl}/^{203}\mathrm{Tl}_{\mathrm{sample}} - {}^{205}\mathrm{Tl}/^{203}\mathrm{Tl}_{SRM997}\right) / \left(^{205}\mathrm{Tl}/^{203}\mathrm{Tl}_{SRM997}\right) \quad (1)$$

The uncertainty of the Tl isotope measurements is estimated to be ~0.5 ε^{205}Tl-units (Nielsen et al., 2004). Thallium procedural blanks were <3 pg throughout this study, which is insignificant compared to the amounts of Tl processed (>5 ng).

3. THALLIUM ISOTOPES IN PYRITES OF THE CARIBBEAN AND THE NORTHEAST PACIFIC

3.1. Confirmation of pyrite in sample solutions

The thallium isotope and chemical compositions of the Late Neogene pyrite samples are listed in Table 1. Even though the sediment cores targeted were described as containing abundant pyrite (Sigurdsson et al., 1997; Lyle et al., 1998a,b), the oxidized nature of the samples precluded macroscopic verification that the separated material was, in fact, pyrite. However, a comparison of the chemical compositions of the supposed pyrite and non-pyrite reference sample reveals several significant indications that the oxidized material was originally pyrite. Firstly, it is evident that all pyrite samples are enriched in Fe by more than a

Table 1
Trace element and Tl isotope composition of Late Neogene pyrites.

	1000A 19H7 40–42 cm	1000A 37 × 4 132–134 cm	1000A 45 × 2 84–86 cm	1020B 3H2 68–70 cm	1020B[a] 3H2 68–70 cm	1020B 23 × 1 40–42 cm	1021B[b] 15H3 89–91 cm	1227D[c] 4H2 41–43 cm
Age (Ma)	4.5	8.5	10.5	0.3	0.3	2.5	0–4	2.5–3.5
Acc. Rate (m/Myr)	37	37	47	113	113	113	20–40	30
Fe	126800	114300	95800	375800	367300	57300	na	2300
Mg	17000	6900	4800	14900	2800	1800	na	850
Ca	14100	84400	37800	3100	830	66400	540	179600
Na	14000	7900	7100	12100	1400	1000	na	460
K	2600	2200	2100	20900	3000	840	na	720
Li	104	24	15.4	27	4.3	5.1	4.8	3.7
Mn	59	67	29	524	220	123	na	16.9
Co	12.7	26	21	12.6	3.6	2.7	22	0.5
Ni	91	244	236	75	237	48	178	9.6
Cu	38	22	13.3	143	219	10.3	196	9.4
Rb	6.4	6.3	6.7	26	8.6	4.7	3.5	4.3
Sr	1260	2200	1300	39	10.6	130	20	800
Cs	0.29	0.4	0.4	1.9	0.7	0.4	0.06	0.8
Ba	136	163	193	281	72	34	63	15.8
Hf	0.5	0.5	0.23	0.14	0.06	0.03	0.08	0.02
Tl	0.14	0.30	0.21	0.22	0.31	0.19	2.7	0.08
Pb	11.4	22	5.5	18.1	2.1	2.2	4.4	1.0
Th	4.0	7.9	62	4.6	0.4	0.28	1.6	0.4
U	3.2	1.5	23	1.0	0.19	1.0	1.0	1.7
ε^{205}Tl	−1.0	1.5	−0.2	0.6	0.8	1.5	2.0	−5.3

All concentrations in ppm. na – not analyzed.
[a] Least oxidized pyrite sample.
[b] Pyritized wood sample.
[c] Pyrite free reference sample.

factor of 20 compared with the non-pyrite sample (Table 1), which is consistent with the presence of an easily dissolvable Fe-bearing mineral. Secondly, all pyrite samples are significantly enriched in cobalt (Co), nickel (Ni) and, to some degree, copper (Cu). Co, Ni and to a lesser extent Cu have been shown to become incorporated significantly into early diagenetic pyrite (Huerta-Diaz and Morse, 1992; Morse and Luther, 1999) and are thus good indicators of this mineral. Co and Ni are also highly enriched in Fe–Mn oxyhydroxides and there is generally more Mn in the pyrite samples than the pyrite-free reference sample (Table 1). However, there is no correlation between Mn and Co or Ni contents as would be expected if Mn oxides were controlling the budget of these trace elements. For example, sample 165-1000A-45x-2, 84–86 cm exhibits almost the same Mn abundance as the reference sample, whereas Co and Ni are highly enriched. Thallium is also highly enriched in Fe–Mn oxy-hydroxides (Hein et al., 2000; Rehkämper et al., 2002), and these minerals could hence account for some of the Tl recovered. However, as is the case for Ni and Co there is no correlation between Mn and Tl concentrations ($r^2 = 0.1$, Table 1) and we infer that Fe–Mn minerals were no longer present in the sediment hosting the pyrite samples.

There is also no systematic difference in the abundances of Ni and Co between the least oxidized pyrite samples from ODP Site 1020B and ODP Site 1021B (pyritized wood) and the other more oxidized samples, suggesting that little element mobilization occurred in storage during the oxidization process. This is also the case for Tl concentrations recorded for the two samples from Hole 1020B that are variably oxidized. We therefore conclude that most of the Fe, Co, Ni and Tl observed for each of the oxidized samples originated from pyrite.

3.2. Potential Tl contamination during sample digestion

The present study is the first to report Tl concentration and isotope data on early diagenetic sedimentary pyrite. Because most of the Late Neogene pyrite samples contained significant detrital material that could have been partially digested in the 8 M HNO_3 used to extract the pyrite, it is difficult to ascertain how much of the Tl in each of the sample solutions was from pyrite as opposed to other minerals. Geochemically Tl is similar to the alkali metals K, Rb and Cs (Shaw, 1952), which bring about strong Tl enrichments in micas and K-feldspar. On the other hand, Tl is highly depleted in biological material such as carbonate (Nielsen and Rehkämper, 2011). The amount of Tl leached from the host sediment during the pyrite digestion procedure will therefore be strongly dependent on the lithological composition of the sediment that hosted the Late Neogene pyrite as well as the mass ratio between pyrite and the other minerals after mechanical separation. Because the lithostratigraphy (especially the relative proportions of biogenic and detrital material) of the sediments at ODP Sites 1000A, 1020B and 1021B can vary substantially (Sigurdsson et al., 1997; Lyle et al., 1998a,b) we will not attempt to estimate the amount

of Tl contamination from host sediment. However, in the following we outline five arguments that indicate that the Tl isotope compositions measured in the Late Neogene pyrite separates closely resemble true pyrite compositions.

(1) Labile sediment components (e.g. Fe–Mn oxy-hydroxides) that could have been dissolved with the pyrite during the acid treatment of the samples were most likely mobilized into sediment porewaters during diagenesis and subsequently partially re-precipitated as pyrite. These components are therefore unlikely to be present in large quantities in the sediments hosting pyrite. This inference is supported by the lack of correlation between Tl and Mn, which indicates that Fe–Mn oxy-hydroxides are no longer present in these sediments.
(2) Partial dissolution of residual detrital grains would be characterized by $\varepsilon^{205}\mathrm{Tl} \sim -2$ (Nielsen et al., 2005). Therefore, mild (<20–30% of total Tl extracted from each sample) contamination with this component would not shift the measured Tl isotope compositions significantly.
(3) Samples from the ODP Hole 1020B exhibit a large range in Fe concentrations (5.7–37%). Pure pyrite contains ~46% Fe and hence the most iron-rich samples must contain little else except pyrite, while the depleted sample could potentially have a large component from the host sediment. However, there is no discernible Tl isotope difference between these samples, which indicates that the potential contaminant did not significantly alter the pyrite Tl isotope composition.
(4) All three ODP Sites from which we have analyzed pyrite contain abundant biogenic material through most of the cored intervals (Sigurdsson et al., 1997; Lyle et al., 1998a,b). Because biogenic sediments contain very little Tl (Nielsen and Rehkämper, 2011) it is unlikely that dissolution of carbonate and leaching of biogenic silica contributed significant amounts of this element. The dilution with biogenic material could also go some way to explain the lower Fe contents in some of the pyrite samples (Table 1).
(5) Potential remobilization of Tl during oxidation in storage appears to be relatively minor (see Section 3.1). In addition, no isotope difference is observed between least and most oxidized samples (Table 1), which strongly indicates that if Tl was somewhat remobilized during storage then it was not associated with any isotopic fractionation.

It is notable that the Tl isotope composition of the pyrite-free sample is significantly lighter than the value of $\varepsilon^{205}\mathrm{Tl} \sim -2$ that would be expected for partial dissolution of detrital material (Table 1). This effect could be explained if stable isotope fractionation occurred during the partial dissolution process. Such a process, however, is not very likely as previous silicate acid leaching procedures were found to cause limited Tl isotope fractionation (Nielsen et al., 2009b). In addition, Schauble (2007) has shown that any significant equilibrium Tl isotope fractionation can only occur in environments where the two Tl valence states (Tl^{+} and Tl^{3+}) are present. In these cases, oxidized Tl is always isotopically heavier than reduced Tl. Since the leaching procedure was conducted using a highly oxidizing solution (8 M HNO_3), and univalent Tl is dominant in silicate minerals (Shaw, 1952), stable isotope fractionation should manifest itself through positive ε^{205}Tl-values in the leachate. Such a circumstance is opposite to the observed effect and thus we conclude that little isotope fractionation occurred during the sediment leaching procedure. More likely, the light isotope composition in the non-pyrite sample is due to dissolution/mobilization of sediment component(s) enriched in ^{203}Tl. The pyrite-free sample did not contain large amounts of Tl so even though biological material has low Tl concentrations (Nielsen and Rehkämper, 2011) it is conceivable that this component could have contributed to the Tl isotope composition of this sample. The high Ca concentrations (Table 1) and abundant diatoms reported for this site (D'Hondt et al., 2003) may explain at least some of the recovered Tl. In addition, Tl initially sorbed onto clay minerals while suspended in the water column (Matthews and Riley, 1970) could also have been released during the leaching procedure. It is unclear what the Tl isotope compositions of the two above-mentioned components are. The ultimate source of Tl is seawater in both cases ($\varepsilon^{205}\mathrm{Tl} \sim -5.5$) and, because neither process is likely to be associated with a change in Tl oxidation state, it follows that the Tl isotope composition of both components are expected to be similar to seawater.

Given the arguments (1–5) outlined above it appears that contamination of the pyrite samples with biological and clay-bound Tl was relatively minor. The lower value of $\varepsilon^{205}\mathrm{Tl} = -1$ recorded for sample 1000A 19H7 40–42 cm also coincides with the lowest Tl concentration, which would make it the most prone to minor amounts of non-pyrite Tl added through the pyrite dissolution procedure. Pyrite from this sample may thus be characterized by a somewhat heavier isotope composition, which would make it more similar to the other Neogene pyrite samples. In general, we cannot exclude the possibility that some of the samples were contaminated by minor amounts of lithogenic, biogenic or clay-sorbed Tl, which, based on the isotope composition measured for the pyrite-free sample, could indicate that the true pyrite isotope compositions are slightly heavier than what is recorded in Table 1. Combining all the above arguments, we conclude that the Tl isotope composition of Late Neogene early diagenetic pyrite from oxic depositional environments is in the range of $\varepsilon^{205}\mathrm{Tl} \sim 0$–3.

3.3. Sources of thallium in Neogene pyrite

The major constituents of marine early diagenetic sedimentary pyrite (Fe and S) come from labile iron associated with sedimentary particles (for example Fe-oxy-hydroxides) and reduction of seawater sulfate (Berner, 1984). Since the Tl concentration of seawater is only ~10–15 pg/g (Flegal and Patterson, 1985; Rehkämper and Nielsen, 2004; Nielsen et al., 2006) it is unlikely that pyrite acquires much

Tl directly from seawater. Instead, it is well known that Tl is strongly adsorbed onto Fe–Mn oxy-hydroxides and also somewhat onto clay minerals (Matthews and Riley, 1970; Shaw, 1952; Turner et al., 2010). These phases are very common in marine sediments and may, during burial and subsequent bacterial reduction of the sediment pore waters, dissociate or desorb some of the adsorbed elements. It is therefore most likely that the Tl enrichment in pyrite originates from these minerals.

This interpretation is also consistent with the isotope compositions inferred for Late Neogene pyrite. Authigenic Fe–Mn oxy-hydroxides that precipitate from seawater are highly enriched in Tl and display very heavy isotope compositions of $\varepsilon^{205}Tl \sim 5$–15 (Rehkämper et al., 2002). Most other materials, for example dissolved and particulate Tl in rivers, display a relatively uniform value of $\varepsilon^{205}Tl \sim -2$ (Nielsen et al., 2005). Continental margin sediments are likely to contain riverine labile Tl ($\varepsilon^{205}Tl \sim -2$), Fe–Mn mineral associated Tl ($\varepsilon^{205}Tl \sim 5$–15) and potentially also seawater Tl adsorbed onto clay minerals ($\varepsilon^{205}Tl \sim -6$), though Tl only sorbs weakly onto clay minerals in normal marine conditions (Turner et al., 2010). Based on these arguments, we conclude that sediment pore waters from which pyrite would precipitate most likely display $\varepsilon^{205}Tl > -2$. Such values are fully consistent with the current measurements.

It cannot be ruled out that some Tl isotope fractionation occurs between pyrite and sediment pore waters. As discussed in Section 3.2., both valence states of Tl are required to generate substantial equilibrium Tl isotope fractionation (Schauble, 2007) and, since Tl^{3+} is highly unlikely to exist under the reducing conditions required for pyrite precipitation, isotope fractionation between pyrite and sediment pore water is probably a minor effect. All the thallium isotope variation observed in the young pyrite samples may be explained via differences in the relative proportions that each of the three components outlined above have contributed to the pyrite. Such variations could be caused by changing the sediment provenance, for example via increased deposition of riverine particles that have labile Tl with $\varepsilon^{205}Tl \sim -2$ (Nielsen et al., 2005). Another mechanism could be variations in sediment depositional rates, whereby low sedimentation rates may result in a larger relative proportion of Tl bound to Fe–Mn minerals if the authigenic flux to the sediment remains unperturbed. However, in the present samples there does not appear to be any relation between sediment accumulation rate and Tl isotope composition of pyrite (Table 1).

3.4. Effect of wood on the thallium isotope composition and concentration of pyrite

In the following section we discuss the potential effect that lack of separation between pyrite and the wood with which it is associated may have on the Tl isotope analyses. This matter is important for the discussion of the Toarcian pyrite because all the samples from Peniche (except one) were processed as a mixture of wood and pyrite, whereas the Port Mulgrave samples were pure pyrite. Hence, if the presence of wood in the Peniche samples induced an isotope effect, an artificial systematic difference between the Peniche and Port Mulgrave samples could have been generated. First, we can compare the modern sample from ODP Site 1021 that contained wood with the other Late Neogene pyrite samples (Table 1). It is evident that the Tl concentration in the wood sample is about an order of magnitude higher than the other samples, suggesting that somehow organic matter may serve to accumulate large quantities of Tl. Importantly, however, this relative enrichment has not generated a significantly different Tl isotope composition because the wood sample shows $\varepsilon^{205}Tl$ indistinguishable from the other Late Neogene samples.

Secondly, as described in Section 2.2, we were able to separate pure pyrite mechanically from one Peniche sample (PW69) and compare the isotope composition to that obtained for pyrite disseminated in wood. The results of this test are outlined in Table 2. It is clear that, within the estimated uncertainty of ± 0.5 $\varepsilon^{205}Tl$-units there is no detectable difference between the two separation methods. Similarly to what is observed for the Late Neogene pyritized wood sample, the concentration of Tl in the PW69 pyrite is very high, again suggesting that organic matter could be responsible for Tl accumulation in the sediment. A further comparison with the Tl concentrations in the remaining wood-rich samples from Peniche is not possible because no attempt was made to quantify the Tl concentrations in these pyrite samples due to the large amounts of wood. However, based on a qualitative assessment of Tl yields for the samples from Peniche, all samples have Tl contents significantly higher than 2 ppm. Thus, there is some evidence to suggest that Tl may accumulate in sediments when associated with organic matter. Whether this implies that Tl is more efficiently incorporated into pyrite or perhaps precipitated as a thallium sulfide is not possible to determine at the present time.

4. THALLIUM ISOTOPES IN TOARCIAN PYRITE

4.1. Results

The thallium isotope compositions of Peniche and Port Mulgrave pyrite are shown in Tables 3 and 4, respectively. Potential contamination with Tl from non-pyrite material during sample dissolution is not likely since the pyrite was relatively simple to isolate from the sediment matrix (except for fossil wood in the Peniche samples). All isotope compositions of the T-OAE samples are therefore assumed to represent pyrite.

At Peniche, large variations in $\varepsilon^{205}Tl$ are apparent throughout the section with a total range of $\varepsilon^{205}Tl = -5.4$ to +6.4, though most of the samples cluster around values

Table 2
Thallium isotope comparison of pyrite separation techniques.

	Analysis 1	Analysis 2	$\varepsilon^{205}Tl$ (ave)	Tl (ppm)
PW69 chemical	−0.1	−0.2	−0.2	nd
PW69 Mechanical	0.3	0.6	0.5	64

nd – Not determined.

Table 3
Thallium isotope composition of Peniche pyrite.

Sample	ε^{205}Tl	Strat. height (cm)	Rel. strat. height[a]	Age (Ma)[b]
PW111	−2.6	3345	3.81	181.645
PW242	−0.5	3241	3.74	181.698
PW103	−4.7	3106	3.64	181.767
PW98	1.9	2817	3.45	181.877
PW95	1.2	2761	3.41	181.896
PW93	1.1	2703	3.37	181.915
PW74	−5.4	2528	3.25	181.975
PW219	−0.9	2454	3.20	182.000
PW72	0.1	2389	3.16	182.022
PW69	0.2	2294	3.09	182.054
PW44	0.5	2196	3.02	182.088
PW88	0.5	2086	2.93	182.140
PW43	6.4	2086	2.93	182.140
PW82	−0.9	1898	2.75	182.242
PW83	4.4	1891	2.74	182.245
PW85	2.5	1891	2.74	182.245
PW81	2.9	1774	2.63	182.309
PW35	2.4	1691	2.55	182.354
PW31	−2.0	1466	2.33	182.475
PW21	0.4	1269	2.14	182.578
PW23	2.2	1168	2.05	182.627
PW22	1.5	1148	2.03	182.637
PW2	−2.2	731	1.68	182.774
PW53	0.3	454	1.43	182.856
PW52	−1.1	452	1.43	182.857
PW4	0.7	448	1.43	182.858
PW5	0.7	350	1.34	182.887
PW14	1.6	249	1.25	182.917
PW18	−1.0	39	1.06	182.979

[a] Relative stratigraphic height is based on the four horizons defined by Hesselbo et al. (2007) that can be correlated between Peniche and Yorkshire. Linear sedimentation rates were assumed in between each horizon.

[b] Ages are based on the orbitally tuned model of Suan et al. (2008) where the absolute age of the Toarcian–Pliensbachian boundary (Horizon 1) is fixed at 183 Ma (Ogg et al., 2008). In addition, it is assumed that the intervals between horizons 1 and 2 as well as between relative stratigraphic heights 3.6 and 4 have durations of ~300 kyr.

Table 4
Thallium isotope composition of Port Mulgrave pyrite.

Sample	ε^{205}Tl	Tl (ppm)	Strat. height (cm)	Rel. strat. height[a]	Age (Ma)[b]
PM2	−1.9	0.62	485	3.91	181.570
PM4	−2.4	0.78	445	3.78	181.664
PM5	−2.5	0.90	425	3.72	181.711
PM6	−2.7	0.16	405	3.66	181.758
PM7	−3.7	0.21	385	3.59	181.803
PM8	−3.8	0.59	365	3.53	181.834
PM11	−3.2	0.17	315	3.38	181.913
PM14	−5.8	0.12	265	3.22	181.991
PM17	−3.4	0.19	215	3.06	182.069
PM18	−3.4	0.12	205	3.03	182.084
PM19	−6.2	0.26	195	3.00	182.100
PM1	−4.5	0.30	180	2.97	182.118
PM24	−6.4	0.12	88	2.77	182.229
PM26	−7.8	0.32	48	2.69	182.277
PM29	−4.5	0.30	8	2.60	182.325
PM30	−5.3	0.14	−12	2.56	182.349
PM31	−3.5	0.23	−32	2.51	182.373
PM32	−3.1	0.21	−52	2.47	182.398
PM33	−2.5	0.22	−72	2.43	182.422
PM35	−3.0	0.20	−102	2.36	182.458
PM36	−5.3	0.36	−112	2.34	182.470
PM37	−5.8	1.44	−132	2.30	182.494
PM39	−6.3	1.54	−172	2.21	182.542

[a] Relative stratigraphic height is based on the four horizons defined by Hesselbo et al. (2007) that can be correlated between Peniche and Yorkshire. Linear sedimentation rates were assumed in between each horizon.

[b] Ages are based on the orbitally tuned model of Suan et al. (2008) where the absolute age of the Toarcian–Pliensbachian boundary (Horizon 1) is fixed at 183 Ma (Ogg et al., 2008). In addition, it is assumed that the intervals between horizons 1 and 2 as well as between relative stratigraphic heights 3.6 and 4 have durations of ~300 kyr.

between ε^{205}Tl = −1 and +2. The average isotope composition of the section is ε^{205}Tl = +0.3. Port Mulgrave pyrite samples have significantly different and less variable Tl isotope compositions. All samples display low ε^{205}Tl-values, ranging from ε^{205}Tl = −7.8 to −1.9, with an average value of ε^{205}Tl = −4.2.

Fig. 2 shows the Tl isotope profiles for Peniche and Yorkshire as well as the concomitant positive and negative carbon isotope excursions (CIE). In both profiles, the Tl isotope variation occurs throughout the Early Toarcian CIE. Since we have not analysed significant numbers of samples bracketing the T-OAE it is unclear whether or not the event is characterized by a Tl isotope anomaly, but the few samples analysed from Peniche, which pre-date the event, show no particular offset from T-OAE samples (Fig. 2A).

We can correlate the two sections stratigraphically by using the four horizons identified by Hesselbo et al. (2007) as present in both Yorkshire and Portugal, based on biostratigraphy and carbon isotope stratigraphy. By assuming constant sediment deposition rates in between each horizon we can define the stratigraphic position of all samples (Tables 3 and 4). We have also fixed the stratigraphic positions to an absolute time scale by implementing the orbitally tuned model of Suan et al. (2008) for the duration of the T-OAE, while utilizing 183 Ma as the age of the Pliensbachian–Toarcian boundary (Ogg et al., 2008), which is defined as horizon 1 (Hesselbo et al., 2007). It should be noted that the assumption of constant sedimentation rate between each horizon is an approximation. With this in mind, it is evident that cross correlation of the two sections is most reliable close to each of the four horizons (dashed lines in Fig. 2) and most uncertain mid-way between horizons. Hence, it is possible that the relative stratigraphic positions could be offset somewhat from values outlined in Tables 3 and 4.

The main observation for the correlated sections is that for large parts of the T-OAE the Tl isotopes in Peniche are offset to values ~4–6 ε^{205}Tl units heavier than Port Mulgrave (Fig. 3). But considering the uncertainties in the

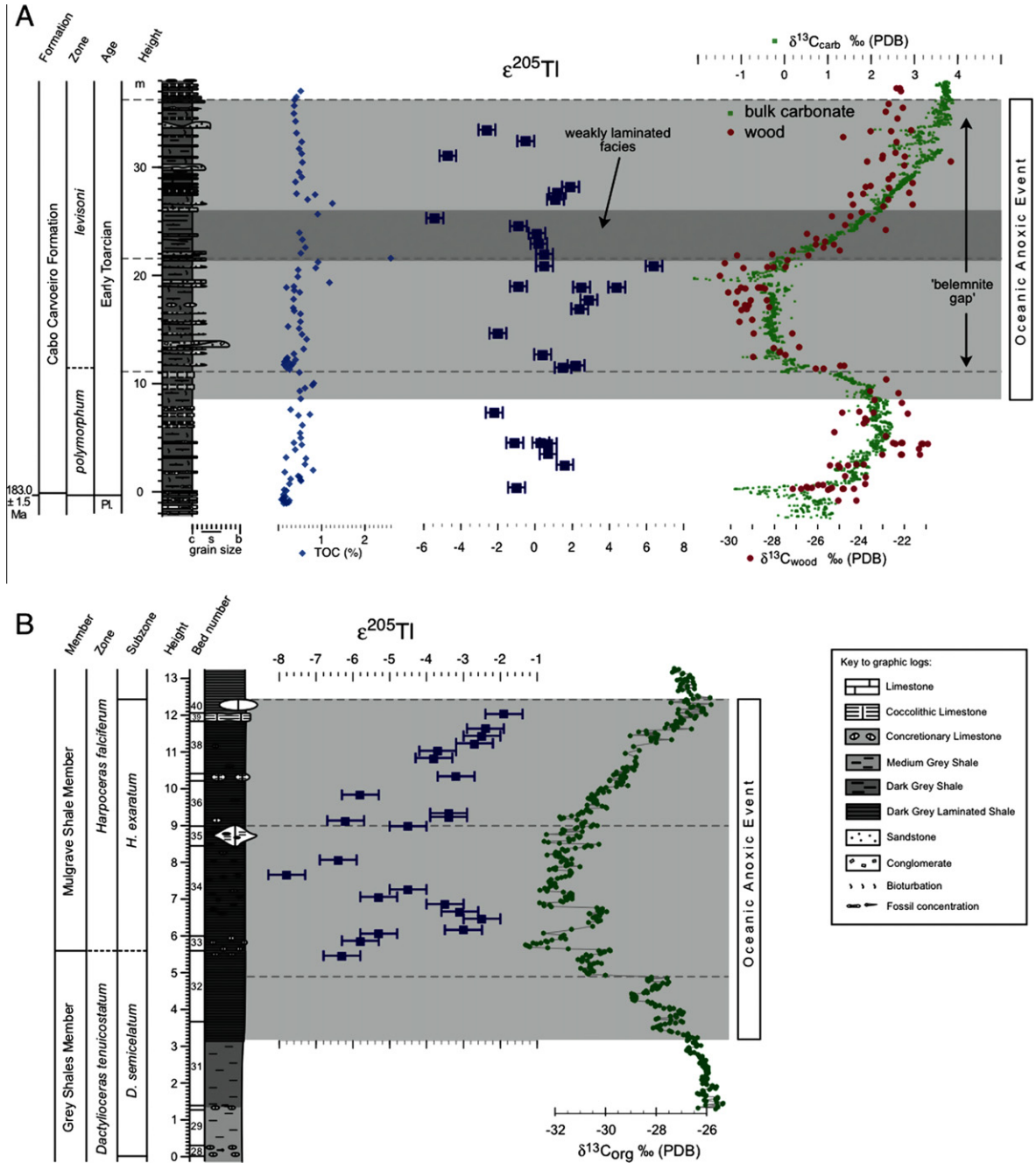

Fig. 2. Carbon isotopes, Tl isotopes, and Tl concentrations (only for Port Mulgrave) for samples from Peniche, Portugal (A) and Port Mulgrave, Yorkshire, UK (B). Carbon isotopes are from Kemp et al. (2005) and Hesselbo et al. (2007).

stratigraphic correlation between the two sites in combination with the relatively coarse sampling density, it is not possible to determine if the two Tl isotope records co-vary or not (Fig. 3).

4.2. Origin of thallium isotope signatures in T-OAE pyrite

The observed Tl isotope signatures could either be a primary signal incorporated during pyrite formation or due to some form of alteration that occurred much later, which presumably caused the systematic offset in average Tl isotope composition between the two sets of pyrite. For example, it is conceivable that fluids percolating through the sediments during tectonic displacement could have caused such late-stage alteration. Accompanying the Tl isotope shift in the pyrite, it might be expected that this process would also have affected other geochemical parameters, in particular molybdenum isotopes, which are strongly associated with pyrite. Other geochemical indices that could be altered are iron and manganese concentrations, which may

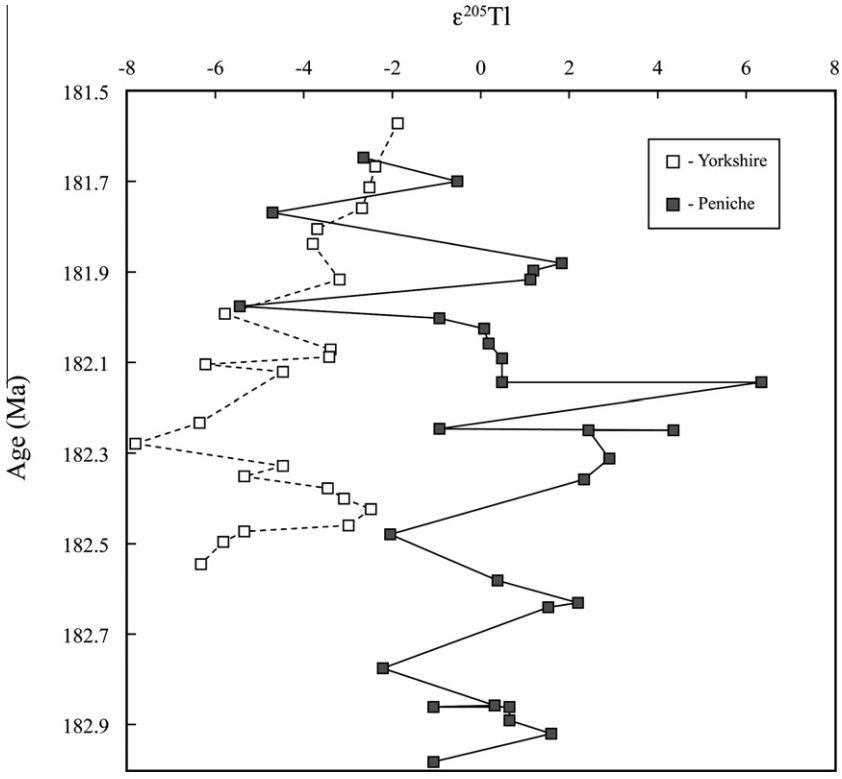

Fig. 3. Correlation between Tl isotopes in early diagenetic pyrite from Peniche and Port Mulgrave. For most of the T-OAE the two sections are offset from each other by ~5 ε^{205}Tl-units. This relationship would be consistent with different redox conditions at the sediment-water interface, where the most positive Tl isotope compositions reflect more oxic conditions (see text for details).

also easily be mobilized by fluid flow. However, there is no indication that any of these geochemical parameters were significantly altered at either Yorkshire or Peniche (Pearce et al., 2008; Hermoso et al., 2009b). It, therefore, seems unlikely that alteration processes caused significant resetting of the Tl isotope compositions of the investigated pyrite samples.

Due to the limited isotope fractionation occurring between sediment pore water and pyrite (as discussed in Section 3.2), the Tl isotope variation was probably controlled either by changes in the isotope compositions or relative importance of the components supplying Tl to the pyrite. For the Late Neogene pyrite, we inferred that the former presence of authigenic marine Fe–Mn oxy-hydroxides with heavy Tl isotope compositions caused the pyrites to inherit ε^{205}Tl-values between 0 and +3. This range of values encompasses almost all samples from Peniche and since there is no other known terrestrial Tl reservoir with heavy Tl isotope compositions, it is reasonable to conclude that the paleoenvironment at Peniche supported significant precipitation of Fe–Mn oxy-hydroxides at the sediment-water interface. These minerals were released diagenetically into the sediment pore waters under reducing conditions, thus giving rise to the observed heavy Tl isotope compositions in the pyrite. This proposed model is consistent with a previous study, which concluded that almost the entire section at Peniche was deposited from a water column whose redox environment was not oxygen depleted enough to cause reduction of oxidized Mn species (Hermoso et al., 2009b).

If interpreted similarly to the Peniche section, the very low ε^{205}Tl-values recorded for the Port Mulgrave pyrite are consistent with sediment deposition occurring with little or no authigenic Fe–Mn oxy-hydroxide precipitation. This effect would result in pyrite acquiring a Tl isotope composition somewhere between continental input fluxes ($\varepsilon^{205}\text{Tl} \sim -2$) and seawater, which at present has an isotope composition of $\varepsilon^{205}\text{Tl} \sim -5.5$ (Rehkämper et al., 2002; Nielsen et al., 2004, 2006). Lack of authigenic Fe–Mn oxy-hydroxide mineral precipitation is also in agreement with the inferred sulfidic conditions in the water column at Yorkshire (Wignall et al., 2005; Bowden et al., 2006), because Fe–Mn oxy-hydroxides require significant oxygenation at the sediment-water interface in order to precipitate. The light isotope composition for the Yorkshire pyrite is therefore considered a local effect caused by the highly anoxic/euxinic conditions at this site during the Toarcian OAE. The offset between the two records was then caused by the different redox conditions whereby initial Fe–Mn oxy-hydroxide precipitation at the seafloor was only supported at Peniche.

In this context, it is interesting to note that there are three samples from the top of the Peniche section that do not display the consistent positive Tl isotope offset from Port Mulgrave (Fig. 3). At present, we cannot explain these one-sample excursions to negative Tl isotope compositions that are very similar to those observed in Yorkshire. However, one of these samples comes from the top of strata that display a combination of elevated total organic carbon

content and a fabric of small horizontal burrows, interpreted as an interval of dysoxic conditions in the water column (Hesselbo et al., 2007). It is therefore possible that the lower Tl isotope composition is the result of lowered or absent Fe–Mn mineral precipitation during these time periods. It should be noted that the four samples below this stratigraphic level also occur within the interval of inferred lower water column oxygenation (Hesselbo et al., 2007). Although these samples are still positively offset from the Port Mulgrave record, the offset is smaller than for the lower sections (Fig. 3), which might suggest that progressively smaller amounts of Fe–Mn minerals were deposited during sedimentation. Alternatively, since sediment porewaters can migrate vertically it might also be expected that some smoothing of the isotopic offset between the oxic and anoxic Tl isotope boundary occur. This effect could also apply to the other sections of the T-OAE where Tl isotope changes are observed, and underlines the fact that the temporal Tl isotope variations recorded by T-OAE pyrite should be seen as qualitative. There does not appear to be any other Tl isotope shifts that can be directly related to lithological changes in the sediments at either site (Fig. 2) and thus this feature is unique to our current data set.

5. IMPLICATIONS FOR PALEOCEANOGRAPHIC PROCESSES DURING THE T-OAE

5.1. Residence time of Tl during T-OAE

One of the greatest challenges of interpreting chemical data from an OAE is to differentiate between global and local processes. Under normal marine conditions many elements have such long residence times that they display almost complete isotopic homogeneity in the oceans. Registration of isotopic perturbations in these elements can therefore be inferred as global in nature. However, during OAEs, the speciation and hence net solubility of redox-sensitive elements is likely to change, possibly modifying substantially the residence time of such elements in the ocean. This phenomenon complicates the inference of global isotope signatures even for elements such as Mo and U that have very long residence times in the modern, oxic ocean (Algeo, 2004).

As outlined in the introduction, the modern marine residence time for Tl is ~20 kyr (Baker et al., 2009; Rehkämper and Nielsen, 2004), which results in a near-homogenous Tl isotope composition of seawater because present-day ocean mixing timescales are on the order of ~1 kyr. During an OAE, the residence time of thallium is not expected to shorten because Tl^+ is the main oxidation state in the modern oceans (Nielsen et al., 2009a) and therefore Tl does not have a major redox change when oxygen levels in the oceans decline. Thallium could potentially precipitate as a sulfide under reducing conditions but, as shown in Fig. 4, the solubility of Tl_2S is so high that it would require Tl concentrations more than three orders of magnitude higher than present-day seawater to begin Tl_2S precipitation, which is unrealistic. Stabilization of Tl sulfide also depends on the T-OAE seawater sulfur abundance (assuming all SO_4^{2-} is converted to HS^-), which we do not know. However, since pyrite framboids were forming in the water column of the Cleveland Basin where the Yorkshire section was deposited

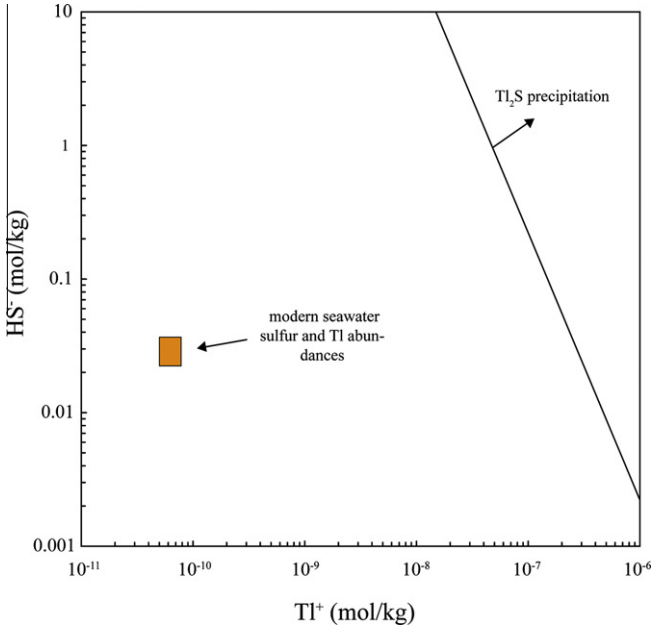

Fig. 4. Thermodynamic equilibrium calculations for the reaction $2Tl^+ + HS^- \rightarrow H^+ + Tl_2S_{(s)}$. Activity coefficients for HS^- ($\gamma = 0.68$) and Tl^+ ($\gamma = 0.63$) were calculated using the methods outlined in Helgeson et al. (1981). Values of the electrostatic Debye–Hückel terms, electrostatic and thermodynamic properties of water and Born solvation coefficients were taken from Helgeson and Kirkham (1974a,b) and Shock et al. (1997), respectively. The HS^- and Tl^+ concentrations plotted for seawater are based on the assumption that total dissolved sulfur and Tl in the Cleveland Basin were similar to modern open ocean values. In addition, it is assumed that all sulfur was present as HS^-. See text for additional details.

(Wignall et al., 2005) it might be more reasonable to expect total sulfur concentrations (predominantly in the form of HS^-) to be lower than the total S concentrations observed in the modern open ocean. We therefore use modern sulfur concentrations as an upper limit for the Cleveland Basin water mass.

Input and/or output fluxes for Tl may have been significantly different in the Jurassic compared with the present day, which would have perturbed the marine residence time. For example, hydrothermal fluid fluxes may have been greater due to higher rates of ocean crust generation (Jones and Jenkyns, 2001) and the warm climate inferred for this period may also have caused increased weathering fluxes from the continents (Cohen et al., 2004). In addition, it is possible that lowered seawater oxygenation during OAEs resulted in decreased Fe–Mn oxy-hydroxide precipitation. All of these factors would have increased the Tl concentration of seawater and thereby lengthened the marine residence time.

It is also possible that authigenic precipitation of pyrite could draw down significant amounts of Tl and thereby alter the marine residence time. We can investigate this by combining the average S/Tl ratio of Yorkshire pyrite (S/Tl $\sim 2 \times 10^6$) with average Jurassic pyrite sulfur burial rates ($\sim 1 \times 10^{13}$ g S/yr) (Berner and Raiswell, 1983). Assuming that all pyrite was authigenic (which is clearly not realistic) this would result in a total Tl flux associated with pyrite of $\sim 5 \times 10^6$ g/yr or 0.025 MMol/yr. Since current Tl input fluxes are on the order of 4 MMol/yr (Fig. 1) and Tl input fluxes may have been even larger during the Jurassic it is very unlikely that authigenic pyrite precipitation affected the marine residence time of Tl appreciably.

Considering these arguments, all evidence points to the conclusion that the Tl isotope composition of seawater was homogenous during the T-OAE and therefore similar at Peniche and Yorkshire. This conclusion underlines the supposition that the observed isotopic offset (Fig. 3) is unlikely to have been caused by different isotope compositions of the water columns at the two sites.

5.2. Control of seawater Tl isotopes during T-OAE

Because the Tl supplied to the pyrite at Port Mulgrave is probably a mixture of only two components, namely continental (ε^{205}Tl $\sim$ -2) and marine, we can use the pyrite to put bounds on the Tl isotope composition of Early Toarcian seawater. Most importantly, Tl isotopes at Port Mulgrave do not increase above a value of $\varepsilon^{205}\mathrm{Tl} = -2$, suggesting that at no point during the T-OAE did seawater increase above this value. Additionally, it is possible that seawater imparted a large portion of the semi-cyclical Tl isotope pyrite variations recorded in the Port Mulgrave pyrites (Fig. 3). This observation indicates that the Tl isotope composition of seawater changed significantly and possibly systematically during the T-OAE. As shown in previous studies, seawater Tl isotopes are most likely controlled by the equation (Nielsen et al., 2009a, 2011):

$$\varepsilon_{SW} = \varepsilon_{IN} - \Delta_{AU} + (\Delta_{AU} - \Delta_{AB})/((F_{AU}/F_{AB}) + 1) \quad (2)$$

Where ε_{SW} and ε_{IN} are the isotope compositions of seawater and the total input fluxes, respectively; Δ_{AU} and Δ_{AB} are the isotopic differences between seawater and authigenic phases and seawater and low-T altered basalts, respectively; and F_{AU}, and F_{AB} are the authigenic and altered basalt output fluxes, respectively. Since ε_{IN} is a constant (Fig. 1) and the isotope fractionations between seawater and the two outputs most likely remained constant over time (Rehkämper et al., 2004; Nielsen et al., 2009a), it is evident that ε^{205}Tl of seawater is controlled primarily by F_{AU}/F_{AB}. Altered basalt fluxes are determined by low-T hydrothermal fluid circulation in cool submarine oceanic crust, which in turn is controlled by the long-term average ocean crust production rate. This parameter can be assumed to be constant on the timescales of an OAE because short-term increases in oceanic crust production such as extrusion of large igneous provinces would only affect low-T hydrothermal circulation during an OAE to a small degree. Therefore, it appears reasonable to conclude that the Tl isotope composition of seawater during the T-OAE was perturbed almost exclusively by variable global Fe–Mn oxy-hydroxide precipitation rates.

Although the Tl isotope composition of seawater was likely homogenous during the T-OAE, the Tl isotope composition of pyrite is not identical to seawater and so we cannot directly use the isotope compositions for Port Mulgrave pyrites to quantitatively assess the changes in marine authigenic precipitation. However, the inferred seawater Tl isotope variations of up to 6 ε^{205}Tl-units would imply that large changes in authigenic Fe–Mn precipitation fluxes during the T-OAE occurred. Specifically, we would predict based on Eq. (2) that decreasing Tl isotope values, as observed from approximately 182.4 Ma to 182.3 Ma (Fig. 3), correspond to decreasing Fe–Mn fluxes.

5.3. Comparison with Mo isotopes

Recently a high-resolution Mo isotope profile was published for the same T-OAE section from Yorkshire (Pearce et al., 2008) as that analysed here for Tl isotopes. The Mo isotope profile reveals four cycles of systematic variations through the Yorkshire section (Fig. 5), which were interpreted to reflect changes in the Mo isotope composition of the global oceans. These cycles of global seawater Mo isotope perturbation were used to calculate that the area of anoxic/euxinic sediment deposition during the T-OAE expanded and contracted, at times covering a total seafloor area more than ten times that of present day. Subsequently, it was shown that the lightest Mo isotope compositions in Yorkshire were indistinguishable from modern riverine input fluxes (Archer and Vance, 2008), which could imply short periods of almost total anoxia/euxinia throughout the global oceans during the T-OAE. Both models would require that for longer or shorter periods during the T-OAE the entire continental shelf suffered euxinic conditions. Such a conclusion is evidently incompatible with our findings here as well as those of Hermoso et al. (2009b), who concluded that the depositional environment at Peniche remained sufficiently oxic for continuous precipitation of Mn oxides to occur for almost the entire T-OAE.

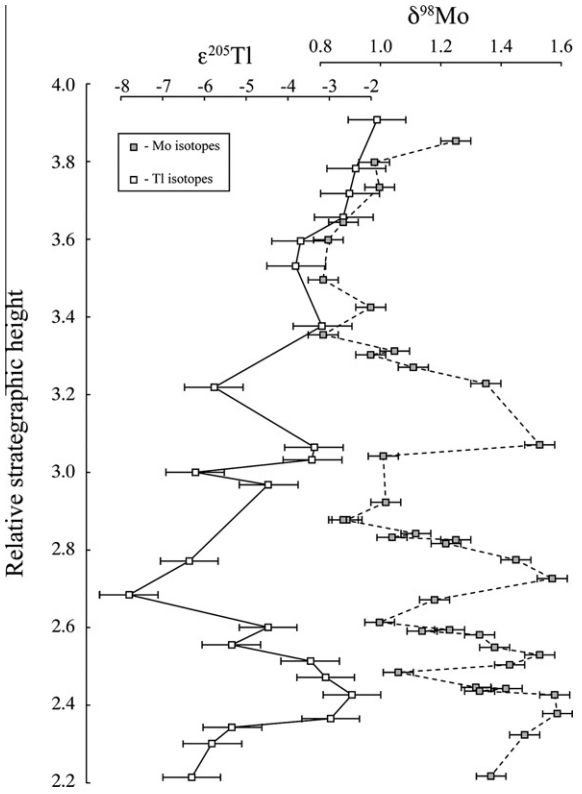

Fig. 5. Comparison of thallium (white squares) and molybdenum (grey squares) isotope compositions measured for pyrites and bulk shales, respectively, at Port Mulgrave, Yorkshire. There is a suggestion that the two isotope systems anti-correlate, which may be consistent with systematic changes in authigenic oxic and anoxic marine outputs. However, the resolution of sampling for the pyrites used for Tl isotope analyses is too coarse to confirm this trend.

Here we compare the Tl and Mo isotope records (Fig. 5) in order to investigate if these isotope proxies responded to common processes and to possibly assess the inference of the very large expansions in anoxic sediment deposition. Based on the comparison shown here, (Fig. 5) it is in principle possible that Tl and Mo isotopes are anti-correlated in the Yorkshire section. Due to the comparatively poor sampling density for Tl isotopes, however, this is difficult to evaluate because several of the cycles evident for Mo isotopes are only covered by a couple of samples in the Tl isotope record.

The marine isotope budgets of Mo and Tl are not controlled by the same external forcing. As shown in Section 5.2., the Tl isotope composition of seawater during the T-OAE was perturbed almost exclusively by variable global Fe–Mn oxy-hydroxide precipitation rates. The marine Mo isotope composition is generally inferred to record changes in the ratio between oxic (Fe–Mn minerals) and anoxic sediment deposition fluxes (Arnold et al., 2004). It is important to note that the areas of oxic and anoxic sediment deposition are not necessarily directly proportional to their respective fluxes. For example, increased marine inputs of Fe and Mn may cause elevated oxic output fluxes that are unrelated to the area of deposition. In this manner Tl and Mo may complement each other very well because Tl only responds to changes in oxic outputs, while Mo responds to both oxic and anoxic outputs.

If we assume that the suggested anti-correlation is correct in combination with the inferred homogenous Tl isotope composition of seawater, then it would imply that the Mo isotopes measured at Yorkshire are likely to represent (or at least are heavily influenced by) the global marine Mo isotope signature. It is still conceivable that the Mo isotope changes are the local expression of the global phenomenon recorded by Tl isotopes. Ultimately, the global signature of the Mo isotope record can only be verified by analyses of Mo isotopes from other euxinic Toarcian localities. Secondly, the interpretation that a decrease in global seawater oxygenation and thereby Fe–Mn oxy-hydroxide precipitation caused the Tl isotope composition of seawater to increase is consistent with the concomitant drop in Mo isotope ratios observed (Fig. 5).

6. CONCLUSIONS AND OUTLOOK

This paper presents the first study of Tl isotopes in early diagenetic pyrite. Measurements from two sections deposited during the Toarcian ocean anoxic event (T-OAE) are compared with data from Late Neogene (<10 Ma) pyrite samples from ODP legs 165 and 167 that were deposited in relatively oxic marine environments.

Our results indicate that early diagenetic pyrite precipitated from sediments originally deposited in an oxic water column display Tl isotope compositions much heavier than seawater. The ^{205}Tl enrichment is due to contributions in the sediment pore waters from Fe–Mn oxy-hydroxides known to adsorb preferentially the heavy Tl isotope (Rehkämper et al., 2002).

In contrast, pyrite in sediments from the Toarcian Cleveland Basin (Yorkshire, UK), which most likely were deposited under euxinic conditions, display Tl isotope compositions that could be more similar to seawater at that time. This observation is consistent with the expected absent Fe–Mn oxy-hydroxide precipitation in a sulfidic water column.

A large Tl isotopic offset between T-OAE sections from Yorkshire and Peniche is interpreted to reflect euxinic and relatively oxic conditions, respectively, during sediment deposition at these two locations. This interpretation is consistent with previous studies of water oxygenation for Peniche and Yorkshire. The inferred difference in water oxygenation at the two sites argues against global marine anoxia during the T-OAE and implies that significant portions of the continental shelf remained oxygenated to some degree.

Thermodynamic calculations of the solubility of Tl_2S and lack of Tl redox change in waters with low oxygen contents strongly suggest that the residence time of Tl during ocean anoxic events, as is the case today, was most likely significantly longer than the ocean mixing time.

Future studies of Tl isotopes in early diagenetic pyrite are needed to confirm whether or not the inferred Tl isotope difference between oxic and anoxic/euxinic environments is indeed correct. Confirmation could, for example, be accomplished via measurements of sedimentary pyrite from the

Black Sea. It will also be important to determine if the Tl isotope composition of pyrites are significantly different in oxic and suboxic environments (as is the case for Mo isotopes).

ACKNOWLEDGEMENTS

We would like to thank Tom Algeo, two anonymous reviewers and AEs Derek Vance and James McManus for their detailed comments, which helped improve this manuscript substantially. Veronique Le Roux is thanked for discussions. SGN is funded by a NERC fellowship. This study used samples provided by the Ocean Drilling Program.

REFERENCES

Al-Suwaidi A. H., Angelozzi G. N., Baudin F., Damborenea S. E., Hesselbo S. P., Jenkyns H. C., Mancenido M. O. and Riccardi A. C. (2010) First record of the Early Toarcian Oceanic Anoxic Event from the Southern Hemisphere, Neuquen Basin, Argentina. *J. Geol. Soc.* **167**, 633–636.

Algeo T. J. (2004) Can marine anoxic events draw down the trace element inventory of seawater? *Geology* **32**, 1057–1060.

Altabet M. A. and Francois R. (1994) Sedimentary nitrogen isotopic ratios as a recorder for surface ocean nitrate utilization. *Global Biogeochem. Cycles* **8**, 103–116.

Archer C. and Vance D. (2008) The isotopic signature of the global riverine molybdenum flux and anoxia in the ancient oceans. *Nat. Geosci.* **1**, 597–600.

Arnold G. L., Anbar A. D., Barling J. and Lyons T. W. (2004) Molybdenum isotope evidence for widespread anoxia in mid-proterozoic oceans. *Science* **304**, 87–90.

Baker R. G. A., Rehkämper M., Hinkley T. K., Nielsen S. G. and Toutain J. P. (2009) Investigation of thallium fluxes from subaerial volcanism – implications for the present and past mass balance of thallium in the oceans. *Geochim. Cosmochim. Acta* **73**, 6340–6359.

Beard B. L., Johnson C. M., Cox L., Sun H., Nealson K. H. and Aguilar C. (1999) Iron isotope biosignatures. *Science* **285**, 1889–1892.

Berner R. A. (1984) Sedimentary pyrite formation – an update. *Geochim. Cosmochim. Acta* **48**, 605–615.

Berner R. A. and Raiswell R. (1983) Burial of organic-carbon and pyrite sulfur in sediments over Phanerozoic time – a new theory. *Geochim. Cosmochim. Acta* **47**, 855–862.

Bidoglio G., Gibson P. N., Ogorman M. and Roberts K. J. (1993) X-ray-absorption spectroscopy investigation of surface redox transformations of thallium and chromium on colloidal mineral oxides. *Geochim. Cosmochim. Acta* **57**, 2389–2394.

Bowden S. A., Farrimond P., Snape C. E. and Love G. D. (2006) Compositional differences in biomarker constituents of the hydrocarbon, resin, asphaltene and kerogen fractions: an example from the Jet Rock (Yorkshire, UK). *Org. Geochem.* **37**, 369–383.

Canfield D. E., Raiswell R. and Bottrell S. (1992) The reactivity of sedimentary iron minerals towards sulfide. *Am. J. Sci.* **292**, 659–683.

Coggon R. M., Rehkämper M., Atteck C. and Teagle D. A. H. (2009) Constraints on hydrothermal fluid fluxes from Tl geochemistry. *Geochim. Cosmochim. Acta* **73**, A234.

Cohen A. S., Coe A. L., Harding S. M. and Schwark L. (2004) Osmium isotope evidence for the regulation of atmospheric CO_2 by continental weathering. *Geology* **32**, 157–160.

D'Hondt S. L., Jørgensen B. B. and Miller C. A., et al. (2003) Site 1227. *Proc. ODP, Init. Rep.* **201**, 1–66.

Emerson S. R. and Huested S. S. (1991) Ocean anoxia and the concentrations of molybdenum and vanadium in seawater. *Mar. Chem.* **34**, 177–196.

Flegal A. R. and Patterson C. C. (1985) Thallium concentrations in seawater. *Mar. Chem.* **15**, 327–331.

Hein J. R., Koschinsky A., Bau M., Manheim F. T., Kang J.-K. and Roberts L. (2000) Cobalt-rich ferromanganese crusts in the Pacific. In *Handbook of Marine Mineral Deposits* (ed. D. S. Cronan). CRC Press, Boca Raton, pp. 239–280.

Heinrichs H., Schulz-Dobrick B. and Wedepohl K. H. (1980) Terrestrial Geochemistry of Cd, Bi, Tl, Pb, Zn and Rb. *Geochim. Cosmochim. Acta* **44**, 1519–1533.

Helgeson H. C. and Kirkham D. H. (1974a) Theoretical prediction of thermodynamic behavior of aqueous electrolytes at high pressures and temperatures. 1: Summary of thermodynamic–electrostatic properties of the solvent. *Am. J. Sci.* **274**, 1089–1198.

Helgeson H. C. and Kirkham D. H. (1974b) Theoretical prediction of thermodynamic behavior of aqueous electrolytes at high pressures and temperatures. 2: Debye–Hückel parameters for activity coefficients and relative partial molal properties. *Am. J. Sci.* **274**, 1199–1261.

Helgeson H. C., Kirkham D. H. and Flowers G. C. (1981) Theoretical prediction of the thermodynamic behavior of aqueous electrolytes at high pressures and temperatures. 4: Calculation of activity coefficients, osmotic coefficients, and apparent molal and standard and relative partial molal properties to 600 °C and 5 Kb. *Am. J. Sci.* **281**, 1249–1516.

Hermoso M., Le Callonnec L., Minoletti F., Renard M. and Hesselbo S. P. (2009a) Expression of the Early Toarcian negative carbon-isotope excursion in separated carbonate microfractions (Jurassic, Paris Basin). *Earth Planet. Sci. Lett.* **277**, 194–203.

Hermoso M., Minoletti F., Le Callonnec L., Jenkyns H. C., Hesselbo S. P., Rickaby R. E. M., Renard M., de Rafelis M. and Emmanuel L. (2009b) Global and local forcing of Early Toarcian seawater chemistry: a comparative study of different paleoceanographic settings (Paris and Lusitanian basins). *Paleoceanography* **24**, PA4208, doi:4210.1029/2009pa001764.

Hesselbo S. P. and Jenkyns H. (1995) A comparison of the Hettangian to Bajocian successions of Dorset and Yorkshire. In *Field Geology of the British Jurassic* (ed. P. D. Taylor). Geological Society, London, pp. 105–150.

Hesselbo S. P., Jenkyns H. C., Duarte L. V. and Oliveira L. C. V. (2007) Carbon-isotope record of the Early Jurassic (Toarcian) Oceanic Anoxic Event from fossil wood and marine carbonate (Lusitanian Basin, Portugal). *Earth Planet. Sci. Lett.* **253**, 455–470.

Huerta-Diaz M. A. and Morse J. W. (1992) Pyritization of trace metals in anoxic marine sediments. *Geochim. Cosmochim. Acta* **56**, 2681–2702.

Jenkyns H. C. (2010) Geochemistry of oceanic anoxic events. *Geochem. Geophys. Geosyst.* **11**, Q03004, doi:03010.01029/02009gc002788.

Jenkyns H. C. and Clayton C. J. (1997) Lower Jurassic epicontinental carbonates and mudstones from England and Wales: chemostratigraphic signals and the early Toarcian anoxic event. *Sedimentology* **44**, 687–706.

Jones C. E. and Jenkyns H. C. (2001) Seawater strontium isotopes, oceanic anoxic events, and seafloor hydrothermal activity in the Jurassic and Cretaceous. *Am. J. Sci.* **301**, 112–149.

Kemp D. B., Coe A. L., Cohen A. S. and Schwark L. (2005) Astronomical pacing of methane release in the Early Jurassic period. *Nature* **437**, 396–399.

Kendall B., Reinhard C. T., Lyons T., Kaufman A. J., Poulton S. W. and Anbar A. D. (2010) Pervasive oxygenation along late Archaean ocean margins. *Nat. Geosci.* **3**, 647–652.

Lyle M., Koizumi I. and Richter C., et al. (1998a) Site 1020. *Proc. ODP, Init. Rep.* **167**, 389–429.

Lyle M., Koizumi I. and Richter C., et al. (1998b) Site 1021. *Proc. ODP, Init. Rep.* **167**, 431–459.

Matthews A. D. and Riley J. P. (1970) The occurrence of thallium in sea water and marine sediments. *Chem. Geol.* **149**, 149–152.

McGoldrick P. J., Keays R. R. and Scott B. B. (1979) Thallium – sensitive indicator of rock–seawater interaction and of sulfur saturation of silicate melts. *Geochim. Cosmochim. Acta* **43**, 1303–1311.

Miller C. A., Peucker-Ehrenbrink B. and Ball L. (2009) Precise determination of rhenium isotope composition by multi-collector inductively-coupled plasma mass spectrometry. *J. Anal. At. Spectrom.* **24**, 1069–1078.

Montoya-Pino C., Weyer S., Anbar A. D., Pross J., Oschmann W., van de Schootbrugge B. and Arz H. W. (2010) Global enhancement of ocean anoxia during Oceanic Anoxic Event. 2: A quantitative approach using U isotopes. *Geology* **38**, 315–318.

Morse J. W. and Luther G. W. (1999) Chemical influences on trace metal–sulfide interactions in anoxic sediments. *Geochim. Cosmochim. Acta* **63**, 3373–3378.

Nielsen S. G., Gannoun A., Marnham C., Burton K. W., Halliday A. N. and Hein J. R. (2011) New age for ferromanganese crust 109D-C and implications for isotopic records of lead, neodymium, hafnium, and thallium in the Pliocene Indian Ocean. *Paleoceanography* **26**, PA2213, doi:2210.1029/2010PA002003.

Nielsen S. G., Mar-Gerrison S., Gannoun A., LaRowe D., Klemm V., Halliday A. N., Burton K. W. and Hein J. R. (2009a) Thallium isotope evidence for a permanent increase in marine organic carbon export in the early Eocene. *Earth Planet. Sci. Lett.* **278**, 297–307.

Nielsen S. G., Prytulak J. and Halliday, A. N. (2011) Determination of precise and accurate 51V/50V isotope ratios by MC–ICP-MS. Part 1: Chemical separation of vanadium and mass spectrometric protocols. *Geostand. Geoanal. Res.* **35**, 293–306.

Nielsen S. G. and Rehkämper M. (2011) Thallium isotopes and their application to problems in earth and environmental science. In *Handbook of Environmental Isotope Geochemistry* (ed. M. Baskaran). Springer, pp. 247–270.

Nielsen S. G., Rehkämper M., Baker J. and Halliday A. N. (2004) The precise and accurate determination of thallium isotope compositions and concentrations for water samples by MC-ICPMS. *Chem. Geol.* **204**, 109–124.

Nielsen S. G., Rehkamper M., Porcelli D., Andersson P., Halliday A. N., Swarzenski P. W., Latkoczy C. and Gunther D. (2005) Thallium isotope composition of the upper continental crust and rivers – an investigation of the continental sources of dissolved marine thallium. *Geochim. Cosmochim. Acta* **69**, 2007–2019.

Nielsen S. G., Rehkämper M., Teagle D. A. H., Alt J. C., Butterfield D. and Halliday A. N. (2006) Hydrothermal fluid fluxes calculated from the isotopic mass balance of thallium in the ocean crust. *Earth Planet. Sci. Lett.* **251**, 120–133.

Nielsen S. G., Williams H. M., Griffin W. L., O'Reilly S. Y., Pearson N. and Viljoen F. (2009b) Thallium isotopes as a potential tracer for the origin of cratonic eclogites. *Geochim. Cosmochim. Acta* **73**, 7387–7398.

Ogg J. G., Ogg G. and Gradstein F. M. (2008) *The Concise Geologic Time Scale*. Cambridge University Press, Cambridge.

Peacock C. L., Moon E. M., Nielsen S. G. and Halliday A. N. (2009) Oxidative scavenging of Tl by Mn oxide birnessite: sorption and stable isotope fractionation. *Geochim. Cosmochim. Acta* **73**, A1003.

Pearce C. R., Cohen A. S., Coe A. L. and Burton K. W. (2008) Molybdenum isotope evidence for global ocean anoxia coupled with perturbations to the carbon cycle during the early Jurassic. *Geology* **36**, 231–234.

Rehkämper M., Frank M., Hein J. R. and Halliday A. (2004) Cenozoic marine geochemistry of thallium deduced from isotopic studies of ferromanganese crusts and pelagic sediments. *Earth Planet. Sci. Lett.* **219**, 77–91.

Rehkämper M., Frank M., Hein J. R., Porcelli D., Halliday A., Ingri J. and Liebetrau V. (2002) Thallium isotope variations in seawater and hydrogenetic, diagenetic, and hydrothermal ferromanganese deposits. *Earth Planet. Sci. Lett.* **197**, 65–81.

Rehkämper M. and Halliday A. N. (1999) The precise measurement of Tl isotopic compositions by MC-ICPMS: application to the analysis of geological materials and meteorites. *Geochim. Cosmochim. Acta* **63**, 935–944.

Rehkämper M. and Nielsen S. G. (2004) The mass balance of dissolved thallium in the oceans. *Mar. Chem.* **85**, 125–139.

Schauble E. A. (2007) Role of nuclear volume in driving equilibrium stable isotope fractionation of mercury, thallium, and other very heavy elements. *Geochim. Cosmochim. Acta* **71**, 2170–2189.

Shannon R. D. (1976) Revised effective ionic radii and systematic studies of interatomic distances in halides and chalcogenides. *Acta Crystallogr., Sect. A* **32**, 751–767.

Shaw D. M. (1952) The geochemistry of thallium. *Geochim. Cosmochim. Acta* **2**, 118–154.

Shock E. L., Sassani D. C., Willis M. and Sverjensky D. A. (1997) Inorganic species in geologic fluids: correlations among standard molal thermodynamic properties of aqueous ions and hydroxide complexes. *Geochim. Cosmochim. Acta* **61**, 907–950.

Siebert C., Nägler T. F., von Blanckenburg F. and Kramers J. D. (2003) Molybdenum isotope records as a potential new proxy for paleoceanography. *Earth Planet. Sci. Lett.* **211**, 159–171.

Sigurdsson H., Leckie R. M., Acton G. D., Abrams L. J., Bralower T. J., Carey S. N., Chaisson W. P., Cotillon P., Cunningham A. D., D'Hondt S., Droxler A. W., Qalbrun B., Gonzalez J., Haug G. H., Kameo K., King J., Lind I. L., Louvel V., Lyons T. W., Murray R. W., Mutti M., Myers G., Pearce R. B., Pearson D. G., Peterson L. C. and Röhl U. (1997) Site 1000. *Proc. ODP, Init. Rep.* **165**, 231–289.

Stirling C. H., Andersen M. B., Potter E. K. and Halliday A. N. (2007) Low-temperature isotopic fractionation of uranium. *Earth Planet. Sci. Lett.* **264**, 208–225.

Suan G., Pittet B., Bour I., Mattioli E., Duarte L. V. and Mailliot S. (2008) Duration of the Early Toarcian carbon isotope excursion deduced from spectral analysis: consequence for its possible causes. *Earth Planet. Sci. Lett.* **267**, 666–679.

Turner A., Cabon A., Glegg G. A. and Fisher A. S. (2010) Sediment–water interactions of thallium under simulated estuarine conditions. *Geochim. Cosmochim. Acta* **74**, 6779–6787.

Wedepohl K. H. (1974) *Handbook of Geochemistry*. Springer.

Wignall P. B., Newton R. J. and Little C. T. S. (2005) The timing of paleoenvironmental change and cause-and-effect relationships during the early Jurassic mass extinction in Europe. *Am. J. Sci.* **305**, 1014–1032.

Wilkin R. T. and Barnes H. L. (1997) Formation processes of framboidal pyrite. *Geochim. Cosmochim. Acta* **61**, 323–339.

Associate editor: James McManus